Submitted to ADVANCED MATERIALS
DOI: 10.1002/adma.((please add manuscript number))

Improving the Stability and Performance of Perovskite Light-Emitting Diodes by Thermal Annealing Treatment

*Jae Choul Yu, Dae Woo Kim, Da Bin Kim, Eui Dae Jung, Jong Hyun Park, Ah-Young Lee, Bo Ram Lee, Daniele Di Nuzzo, Richard H. Friend and Myoung Hoon Song**

[*] Prof. Myoung Hoon Song[+], Jae Choul Yu, Dae Woo Kim, Da Bin Kim, Eui Dae Jung, Jong Hyun Park, Ah-Young Lee
School of Materials Science Engineering and KIST-UNIST Ulsan Center for Convergent Materials, Ulsan National Institute of Science and Technology (UNIST), UNIST-gil 50, Ulsan, 689-798, Republic of Korea
E-mail: mhsong@unist.ac.kr

Prof. Richard H. Friend, Dr Bo Ram Lee, Dr Daniele Di Nuzzo,
Cavendish Laboratory, JJ Thomson Avenue, Cambridge, CB3 0HE, United Kingdom

[+] Current address: Cavendish Laboratory, JJ Thomson Avenue, Cambridge, CB3 0HE, United Kingdom

Keywords: perovskite; perovskite light-emitting diodes (PeLED); long-term stability; electroluminescence (EL)

Organic-inorganic hybrid perovskite materials have attracted the attention of many researchers involved in the field of photovoltaics because of their excellent merits, which include high charge carrier mobility, long-range balanced hole-electron transport, a tuneable optical bandgap, and solution processability.[1-5] The power conversion efficiencies (PCEs) of perovskite solar cells have increased from 3 % to more than 20 % in just a few years, approaching the state-of-the-art performance of thin-film crystalline silicon solar cells.[6-10] Recently, a few reports on perovskite films have demonstrated that they exhibit a narrow-band emission (full-width at half-maximum, FWHM, of approximately 20 nm), a photoluminescence quantum efficiency (PLQE) as high as 70 % at low temperatures, and a higher optical gain for lasing.[11-13] Thus, perovskite materials are regarded as a next-generation candidate for applications in lasers, photodetectors and light-emitting diodes (LEDs).[11-18] In addition, caesium lead halide-based perovskite quantum dots have been intensively studied because of their unique properties, which include a PLQE as high as 95 %, a narrow emission spectrum, and a size-dependent emission wavelength determined by the quantum confinement effect.[19-21] Recently, quantum dot LEDs based on cesium lead halide perovskite ($CsPbX_3$) were firstly reported with a maximum external quantum efficiency (EQE) of 0.12 % for green emission.[22]

Organic-inorganic hybrid perovskites LEDs (PeLEDs) were first reported with a radiance of 6.8 W sr^{-1} m^{-2} and a maximum EQE of 0.76 % for infrared emission and with a luminance of 364 cd m^{-2} and a maximum EQE of 0.1 % for green emission.[12] Recently, improved efficiencies for PeLEDs have been achieved through modification of the hole-transport layer (HTL) and the electron-transport layer (ETL), which reduces the charge-transport barrier between the charge transport layer and the perovskite emissive layer.[23,24] Moreover, the use of composites of a perovskite and a polymer as the emission layer has been demonstrated to result in perovskite films with a uniform morphology and, consequently, in PeLEDs with increased efficiency.[25-27]

So far, the importance of morphology and the quality of perovskite films in the performance of PeLEDs has not yet been systematically studied, even though high crystallinity, excellent morphology and balanced stoichiometry of the perovskite film have been reported to substantially influence the photovoltaic performance of perovskite solar cells.[7, 8, 28, 29] Recently, our group has demonstrated that enhanced performance of PeLEDs prepared using a DMF/HBr co-solvent is achieved through the fabrication of uniform methylammonium lead tribromide ($CH_3NH_3PbBr_3$, $MAPbBr_3$) films with complete surface coverage.[30] Moreover, Cho et al. have reported a highly efficient PeLED with an 8.53 % EQE, using nanograin engineering and a stoichiometric modification of methylammonium bromide (MABr) and lead dibromide ($PbBr_2$).[31] However, the long-term stability of PeLEDs has not been much reported.

Here, we investigated the effect of thermal annealing on the morphology and crystallinity of $MAPbBr_3$ films as well as the performance and long-term stability of PeLEDs. A continuous perovskite film with high crystallinity was fabricated using a thermal annealing treatment. The PeLED with a $MAPbBr_3$ film fabricated under optimized thermal annealing conditions exhibited improved device performance and full coverage of the green electroluminescence (EL) at the turn-on voltage because of the high quality of the continuous perovskite layer, as confirmed by scanning electron microscopy (SEM) and inverted optical microscopy. Moreover, the encapsulated PeLED with the $MAPbBr_3$ film prepared under the optimized thermal annealing conditions exhibited excellent long-term stability under ambient conditions.

Figure 1a shows a schematic of the inverted-structured PeLED (ITO/PEDOT:PSS/$MAPbBr_3$/SPW-111/LiF/Ag), which uses PEDOT:PSS as a HTL, the $MAPbBr_3$ as a green emitter layer, SPW-111 (“White Polymer”, Merck Co.) as an ETL, indium tin oxide (ITO) as an anode, and LiF/Al as a cathode. To obtain uniform and dense $MAPbBr_3$ films, the $MAPbBr_3$ layer used as the emissive layer was deposited onto a

PEDOT:PSS-coated ITO/glass substrate by spin-casting a 1:1 molar ratio solution of $PbBr_2$ and MABr in a DMF/HBr co-solvent.[30] Details of the fabrication of the PeLEDs are described in the experimental section. The energy-level diagrams of the fabricated PeLED are described in **Figure 1**b, and the uniform EL from our optimized PeLED with the $MAPbBr_3$ film annealed at 60 °C for 2 hr is shown in **Figure 1**c.

Annealing is an important process in the formation of the perovskite layer, as it promotes the formation of a perovskite crystal and removes any excess solvent remaining in the film.[28] We have observed that perovskite films stored in an N_2-filled glove box showed an evolution of its morphology over time scales of a week or more. Details of these experiments are reported in the supporting information. Here, we explore how a controlled thermal annealing process would enable the $MAPbBr_3$ to become a continuous perovskite film much more quickly from a kinetics viewpoint. We report below accelerated morphology evolution obtained by annealing at temperatures up to 100 °C.

The influence of thermal annealing on the morphology and composition of the $MAPbBr_3$ films that formed on the PEDOT:PSS-coated ITO/glass substrates was characterized by SEM and energy dispersive spectrometer (EDS), as shown in **Figure 2** and **Table S3**, respectively. The $MAPbBr_3$ films stored at room temperature (RT) for 2 hrs and annealed at 60 °C for 2 hrs showed good coverage of the $MAPbBr_3$ crystals in the top-view SEM images, as shown in **Figure 2**a-b. By contrast, some vertical cracks in the perovskite film stored at RT for 2 hrs were observed in the cross-sectional SEM image, as shown in **Figure 2**e. However, a homogeneous and continuous $MAPbBr_3$ film was obtained after annealing at 60 °C for 2 hrs as observed in the cross-sectional SEM image in **Figure 2**f, because of the induced recrystallization and grain growth in the formed perovskite film subjected to the thermal annealing process.[32-34] However, melted perovskite crystals without the original cubic shape were observed in the top-view SEM image of the perovskite films annealed at 100 °C for 2 hrs, as show in **Figure 2**d. Moreover, the $MAPbBr_3$ films annealed at 80 and 100 °C for 2 hrs

showed vertical cracks in the cross-sectional SEM images (**Figure 2**g-h), whereas the cross-sectional SEM image the $MAPbBr_3$ film annealed at 60 °C for 2 hrs showed a densely connected morphology (**Figure 2**f). The cracks in the $MAPbBr_3$ films (**Figure 2**g, h) may originate from the sublimation of MABr. To explain this hypothesis, EDS was used to quantitatively analyse the $MAPbBr_3$ films prepared under different thermal annealing conditions. The concentrations of Br and C in the $MAPbBr_3$ film annealed at 100 °C for 2 hrs decreased by 150 % compared with those of the $MAPbBr_3$ film annealed at 60 °C for 2 hrs. The detailed concentrations of the components are summarized in **Table S3**. This observation is in good agreement with the top-view and cross-sectional SEM images of the perovskite films annealed at 60 and 100 °C for 2 hrs (**Figure 2**). Consequently, **Figure 2** and **Table S3** show that the thermal annealing conditions substantially influence the morphology of the $MAPbBr_3$ films.

To confirm the enhanced crystallinity of $MAPbBr_3$, we used XRD to characterize the films treated under various thermal annealing conditions (**Figure 3**a). Two distinct diffraction peaks were observed for the (100) (14.95°) and (200) (30.15°) planes, which correspond to $MAPbBr_3$ crystalline peaks. The intensities of the two peaks in the XRD patterns of the $MAPbBr_3$ film annealed at 60 °C for 2 hrs increased by 135 % compared with those of the $MAPbBr_3$ film stored at RT for 2 hrs. This is not surprising: in fact, the method of thermal annealing has been broadly applied in both inorganic and organic films to enhance crystallization and grain growth.[32-34] As the annealing temperature was increased to 100 °C for 2 hrs, the peak intensities dramatically decreased because of the decomposition of $MaPbBr_3$ by sublimation of MABr.

To establish a clear correlation between the annealing conditions of the $MAPbBr_3$ films and the device performance of the PeLEDs, we investigated the current-density vs. voltage (*J-V*), the luminance vs. voltage (*L-V*) and the luminous efficiency vs. luminance (*LE-L*) characteristics of the PeLEDs with $MAPbBr_3$ treated at various annealing temperatures for 2

hrs (**Figure 3**b-d). The figure inset shows the EL spectra of the PeLEDs with $MAPbBr_3$ treated under various annealing conditions, showing approximately the same emission spectra with a FWHM of ~20 nm. The $MAPbBr_3$-based PeLED stored at RT for 2 hrs exhibited a maximum luminance of 2,350 cd m^{-2} (at 4.5 V) and a luminous efficiency of 0.23 cd A^{-1} (at 4.5 V). By contrast, the optimized PeLED with an $MAPbBr_3$ film annealed at 60 °C for 2 hrs exhibited a remarkably enhanced maximum luminance at 7,850 cd m^{-2} (at 5.1 V) and a maximum luminous efficiency of 0.92 cd A^{-1} (at 5.1 V), which represent enhancements of approximately 330 % and 400 %, respectively. However, when the annealing temperature was increased to 80 and 100 °C for 2 hrs, the performance of the PeLEDs decreased, correlating with the formation of vertical cracks in the perovskite films caused by the sublimation of Br and C and the decrease in the crystallinity of the perovskite films. The detailed device performance values of the PeLEDs with an $MAPbBr_3$ film treated under different annealing conditions are summarized in **Table 1**.

Furthermore, PeLEDs with an $MAPbBr_3$ film treated for different annealing times and at different temperatures were fabricated to confirm the detailed correlation between the annealing conditions and the device performance, as shown in **Figures S4-6**. The parameters of the corresponding PeLEDs are summarized in **Tables S4-6**. The overall performance of the PeLEDs with an annealed $MAPbBr_3$ film increased with increasing annealing time until 30 mins. However, the efficiencies of the PeLEDs with an $MAPbBr_3$ film annealed at 80 °C and 100 °C for more than 1 hr decreased substantially. These results are in good agreement with the EDS quantitative analysis, which showed a substantial decrease in the amount of components that contain Br and C, which ultimately degrade the PeLED performance. In the case of thermal annealing for longer than 1 hr, an increase in leakage currents was observed in the *J-V* curves, as shown in **Figure S6**a, which may be due to the discontinuous morphology of the perovskite films with vertical cracks that formed by the more rapid sublimation rate of

the perovskite component in the $MAPbBr_3$ film annealed at a higher temperature for a long time.

We further investigated the effect of thermal annealing on the uniformity of the EL emission in complete PeLEDs with $MAPbBr_3$ annealed at various annealing temperatures for 2 hrs using an optical microscope, as shown in **Figure S7**. Non-uniform EL images of PeLEDs with an $MAPbBr_3$ film annealed at 100 °C and stored at RT for 2 hrs were observed at both 2.5 and 3.7 V, whereas very good coverages in the EL images of the PeLED with an $MAPbBr_3$ film annealed at 60 °C for 2 hrs were observed at both 2.5 and 3.7 V because of the continuous $MAPbBr_3$ film with high crystallinity. In general, the full coverage emission at turn-on and operating voltages is absolutely necessary for commercial display applications. However, the PeLED with an $MAPbBr_3$ film annealed at 100 °C and for 2 hrs showed significantly reduced EL spots, which were attributed to the melted morphology of the $MAPbBr_3$ layer with inhomogeneous compositions caused by the decomposition of Br and C, as shown in **Figure S7**d-h. Consequently, the condition of higher annealing temperatures leads to a remarkable decrease in the performance of devices fabricated with $MAPbBr_3$ films with a non-uniform morphology.

One of the most critical concerns regarding PeLEDs is their long-term stability. For the long-term stability tests, the performance of encapsulated PeLEDs with an $MAPbBr_3$ film treated at various temperatures for 2 hrs was measured at 3.8 V under ambient air conditions, as shown in **Figure 4**a. The long-term stability of the encapsulated PeLEDs was measured at 4 hr intervals; the luminance of the encapsulated PeLEDs was first measured 30 times, and the average value was determined for each device; the tested PeLEDs were then stored in a glovebox for about 4 hrs, representing a single cycle. The measurement procedure was then repeated.

Interestingly, the PeLED with an $MAPbBr_3$ film annealed at 60 °C for 2 hrs showed not only better device performance but also a significantly enhanced long-term stability. However,

a dramatic decrease in the luminance values of the PeLEDs with $MAPbBr_3$ films treated at RT and at 100 °C for 2 hrs was observed after 25 cycles (100 hrs, non-continuous test) and 47 cycles (150 hrs, non-continuous test), respectively; we interpret this behaviour as originating from substantial joule heating due to a large current flow through the crack sites. To confirm the reproducibility of the long-term stability, 15 samples of PeLEDs with $MAPbBr_3$ films prepared under different annealing conditions were measured. In particular, more than 70 % of the PeLED samples with an $MAPbBr_3$ film annealed at 60 °C for 2 hrs maintained their initial luminance values even after 162 cycles (650 hrs, non-continuous test) of operation. **Figure 4**b-c shows the *J-V* and *L-V* characteristics of the PeLEDs with $MAPbBr_3$ films stored at RT and annealed at 60 °C for 2 hrs before and after 47 cycles (150 hrs, non-continuous test) and 162 cycles (650 hrs, non-continuous test) of operation. The PeLED with an $MAPbBr_3$ film stored at RT for 2 hrs showed an increase in the leakage current density and no luminance after 47 cycles (150 hrs, non-continuous test) of operation, whereas the PeLED with an $MAPbBr_3$ film annealed at 60 °C for 2 hrs showed the same *J-V* and *L-V* behaviour even after 162 cycles (650 hrs, non-continuous test) of operation. The increase in leakage current supports our interpretation of the degradation being driven by current flowing through the crack sites: this current generates joule heating and accelerates the sublimation of MABr.

To clarify the influence of morphology on the $MAPbBr_3$ films after long-term device operation, we used SEM to observe cross sections of the complete devices (Glass/ITO/PEDOT:PSS/$MAPbBr_3$/SPW-111/LiF/Ag) before and after operation (**Figure 4**d-f). Disrupted $MAPbBr_3$ films with cracks caused by the joule heating effect are clearly observed after 47 (150 hrs, non-continuous test) and 62 cycles (250 hrs, non-continuous test) of operation in the case of the PeLEDs with $MAPbBr_3$ films stored at RT and annealed at 100 °C for 2 hrs, respectively. However, no change in the morphology of the perovskite film was observed after 162 cycles (650 hrs, non-continuous test) of operation in the case of the PeLED with an $MAPbBr_3$ film annealed at 60 °C for 2 hrs. These results clearly demonstrate

that the device long-term stability increased because of the enhanced thermal stability of the continuous and connected $MAPbBr_3$ film that formed after annealing at 60 °C for 2 hrs. In particular, we were surprised that the PeLEDs with an $MAPbBr_3$ film annealed at 100 °C for 2 hrs exhibited more stable operation than devices with an $MAPbBr_3$ film stored at RT for 2 hrs. This more stable operation may be due to the better connection in the $MAPbBr_3$ film after thermal annealing despite of the presence of vertical cracks in the $MAPbBr_3$ film.

The luminance values of PeLEDs with $MAPbBr_3$ films treated at RT and 60 ^oC and 100 ^oC for 2 hrs were measured under constant bias of 3.4 V for 1 hr. The luminance values of the encapsulated PeLED annealed at 60 °C for 2 hrs decreased by approximately 75 % after 1 hr of continuous DC bias operation, while the PeLEDs with $MAPbBr_3$ films treated at RT and 100 ^oC for 2 hrs showed significantly decreased luminance values after 15 min of continuous DC bias operation because of substantial joule heating from a large current flow through the crack sites, as shown in **Figure S8**a. However, after the PeLED was stored in the glovebox for 4 hrs after operation, the PeLED annealed at 60 °C for 2 hrs exhibited its initial luminance value (approximately 400 cd m^{-2} at 3.4 V), as shown in **Figure S8**b. The recovery of luminance in the PeLED stored in the glovebox for 4 hrs was confirmed by photographs of the EL emission of the PeLED at a 3.4 V bias before and after 1 hr of continuous operation and after storage in the glovebox for 4 hrs (**Figure S9**).

Figure 5 shows optical micrographs of the electroluminescence from operating PeLEDs under a continuous DC bias. Emission is localised on length scales of a few μm, consistent with variations in emission from different crystallites (arising from differences in electron and hole currents reaching each crystallite, or differences in luminescence yield from each crystallite). Under continuous drive, the emission was found to ‘blink’, with individual regions switching between bright and dark reversibly with time. It is likely that this behaviour is associated with ion migration that causes changes in the electrical connectivity between crystallites. However, the detailed mechanism behind the luminance recovery should be

studied further; such investigations are currently underway.

In this work, we investigated the influence of thermal annealing on the morphology of $MAPbBr_3$ films, leading to the improved performance and long-term stability of PeLEDs. In particular, the thermal annealing conditions substantially influenced the morphology and quality of the $MAPbBr_3$ films. The perovskite film annealed at 60 °C for 2 hrs, which were found to be the optimum thermal annealing conditions, exhibited a highly crystalline and continuous morphology without vertical cracks, which was confirmed by SEM, EDS and XRD measurements. The PeLED fabricated using a perovskite film treated under the optimum thermal annealing conditions also exhibited improved device performance, with a maximum luminance of 7,850 cd m^{-2} (at 5.1 V), a maximum luminous efficiency of 0.92 cd A^{-1} (at 5.1 V) and a maximum external quantum efficiency (EQE) of 0.2 %, as well as good coverage of a green EL at the turn-on voltage (at 2.5 V) and the operation voltage (at 3.7 V). Moreover, the encapsulated PeLEDs with a continuous $MAPbBr_3$ film treated under the optimum thermal annealing conditions showed excellent long-term stability, maintaining their initial luminance values even after 162 cycles (650 hrs, non-continuous test) of operation under ambient conditions because of the continuous and highly crystalline morphology of the crack-free perovskite layer. To the best of our knowledge, this study presents the best long-term stability observed in an inverted-structured PeLED. The thermal annealing of the perovskite films in PeLEDs clearly shows a correlation between the morphology of the perovskite layer and the stability of the PeLED, and we believe that it furthers the scientific study of the long-term stability and commercialization of PeLEDs. We also observed the phenomenon of emission blinking from the PeLED in the optical microscope, which indicates that the emission spots changes reversibly with time, and it seems to be related to the migration of ions under a continuous bias.

Experimental Section

Materials. The synthesis of methylammonium bromide (MABr) and the preparation of the methylammonium lead tribromide ($MAPbBr_3$) solution have been described elsewhere.[30] The SPW-111 polymer was purchased from Merck Co. and was used without further purification. All reagents were used as received without further purification: lead bromide ($PbBr_2$, 99 %, Alfa Aesar), methylamine (40 % in methanol, TCI), *N*,*N*-dimethylformamide (DMF, Aldrich), chlorobenzene (Aldrich), and hydrobromic acid (HBr, Aldrich).

Device fabrication. For the fabrication of the inverted-structured PeLEDs, PEDOT:PSS was spin-coated onto a clean ITO-coated glass substrate at 5,000 rpm for 40 s and then annealed at 130 °C for 10 mins. The $MAPbBr_3$ precursor (37.8 wt. % MABr and $PbBr_2$, 1:1 molar ratio in DMF) solution with 6 vol. % HBr aqueous solution was spin-coated onto the PEDOT:PSS-coated electrodes at 3,000 rpm for 60 s and treated at various temperatures (ambient temperature, 60, 80, and 100 °C) for various times (10 mins to 4 hrs) in N_2-filled glovebox. The ETL was coated using SPW-111 dispersed in chlorobenzene (0.55 wt. %). Finally, LiF (1 nm) and silver (80 nm) were deposited successively by the thermal evaporation method. The active area of the device was 13.5 mm^2. The devices were encapsulated before testing.[30]

Characterization of $MAPbBr_3$ films and PeLEDs. SEM (Nanonova 230, FEI) was used to observe the morphology and determine the elemental composition of the $MAPbBr_3$ films. EDS analyses were performed on a Nanonova 230 microscope operated at 10 kV. XRD patterns were obtained from samples of $MAPbBr_3$ films treated at various temperatures (ambient temperature to 100 °C) for 2 hrs after being deposited onto a PEDOT:PSS-coated glass substrate; the patterns were recorded using an XRD (D8 Advance, Bruker) equipped with a Cu Kα radiation source (λ = 1.5405 Å). A step size of 0.01° was chosen, with an acquisition time as high as 5 min deg^{-1}.[30] EL microscope images were obtained from samples of the PeLEDs under a constant applied voltage using an inverted optical microscope (OE, IX81, Olympus). The measurements of encapsulated PeLEDs were performed using a

Keithley 2400 source measurement unit and a Konica Minolta spectroradiometer (CS-2000, Minolta Co.) under ambient air conditions.

Supporting Information

Supporting Information is available online from the Wiley Online Library or from the author.

Acknowledgements

This study was supported by the Mid-Career Researcher Program (2015R1A2A2A01003263). This work was financially supported by the KIST-UNIST partnership program (1.150091.01/2.150464.01). This work was also supported by the Human Resource Training Program for Regional Innovation and Creativity through the Ministry of Education and National Research Foundation of Korea (NRF-2014H1C1A1073051).

Received: ((will be filled in by the editorial staff))
Revised: ((will be filled in by the editorial staff))
Published online: ((will be filled in by the editorial staff))

References

[1] C. Wehrenfennig, G. E. Eperon, M. B. Johnston, H. J. Snaith, L. M. Herz, *Adv. Mater.* **2014**, *26*, 1584.

[2] S. D. Stranks, G. E. Eperon, G. Grancini, C. Menelaou, M. J. P. Alcocer, T. Leijtens, L. M. Herz, A. Petrozza, H. J. Snaith, *Science* **2013**, *342*, 341.

[3] C. S. Ponseca, Jr., T. J. Savenije, M. Abdellah, K. Zheng, A. Yartsev, T. Pascher, T. Harlang, P. Chabera, T. Pullerits, A. Stepanov, J. P. Wolf, V. Sundstrom, *J. Am. Chem. Soc.* **2014**, *136*, 5189.

[4] G. Xing, N. Mathews, S. Sun, S. S. Lim, Y. M. Lam, M. Gratzel, S. Mhaisalkar, T. C. Sum, *Science* **2013**, *342*, 344.

[5] J. H. Noh, S. H. Im, J. H. Heo, T. N. Mandal, S. I. Seok, *Nano Lett.* **2013**, *13*, 1764.

[6] A. Kojima, K. Teshima, Y. Shirai, T. Miyasaka, *J. Am. Chem. Soc.* **2009**, *131*, 6050.

[7] M. Liu, M. B. Johnston, H. J. Snaith, *Nature* **2013**, *501*, 395.

[8] J. Burschka, N. Pellet, S.-J. Moon, R. Humphry-Baker, P. Gao, M. K. Nazeeruddin, M. Gratzel, *Nature* **2013**, *499*, 316.

[9] H. Zhou, Q. Chen, G. Li, S. Luo, T.-b. Song, H.-S. Duan, Z. Hong, J. You, Y. Liu, Y. Yang, *Science* **2014**, *345*, 542.

[10] W. S. Yang, J. H. Noh, N. J. Jeon, Y. C. Kim, S. Ryu, J. Seo, S. I. Seok, *Science* **2015**, *348*, 1234.

[11] F. Deschler, M. Price, S. Pathak, L. E. Klintberg, D. D. Jarausch, R. Higler, S. Huttner, T. Leijtens, S. D. Stranks, H. J. Snaith, M. Atature, R. T. Phillips, R. H. Friend, *J. Phys. Chem. Lett.* **2014**, *5*, 1421.

[12] Z.-K. Tan, R. S. Moghaddam, M. L. Lai, P. Docampo, R. Higler, F. Deschler, M. Price, A. Sadhanala, L. M. Pazos, D. Credgington, F. Hanusch, T. Bein, H. J. Snaith, R. H. Friend, *Nature Nanotech.* **2014**, *9*, 687.

[13] H. Zhu, Y. Fu, F. Meng, X. Wu, Z. Gong, Q. Ding, M. V. Gustafsson, M. T. Trinh, S. Jin,

X. Y. Zhu, *Nature Mater.* **2015**, *14*, 636.

[14] X. Hu, X. D. Zhang, L. Liang, J. Bao, S. Li, W. L. Yang, Y. Xie, *Adv. Funct. Mater.* **2014**, *24*, 7373.

[15] Y. Lee, J. Kwon, E. Hwang, C. H. Ra, W. J. Yoo, J. H. Ahn, J. H. Park, J. H. Cho, *Adv. Mater.* **2015**, *27*, 41.

[16] G. Xing, N. Mathews, S. S. Lim, N. Yantara, X. Liu, D. Sabba, M. Gratzel, S. Mhaisalkar, T. C. Sum, *Nature Mater.* **2014**, *13*, 476.

[17] A. Sadhanala, S. Ahmad, B. Zhao, N. Giesbrecht, P. M. Pearce, F. Deschler, R. L. Z. Hoye, K. C. Gödel, T. Bein, P. Docampo, S. E. Dutton, M. F. L. De Volder, R. H. Friend, *Nano Lett.* **2015**, *15*, 6095.

[18] A. B. Wong, M. Lai, S. W. Eaton, Y. Yu, E. Lin, L. Dou, A. Fu, P. Yang, *Nano Lett.* **2015**, *15*, 5519.

[19] L. Protesescu, S. Yakunin, M. I. Bodnarchuk, F. Krieg, R. Caputo, C. H. Hendon, R. X. Yang, A. Walsh, M. V. Kovalenko, *Nano Lett.* **2015**, *15*, 3692

[20] X. Li, Y. Wu, S. Zhang, B. Cai, Y. Gu, J. Song, H. Zeng, *Adv. Funct. Mater.* http://dx.doi.org/10.1002/adfm.201600109.

[21] G. Nedelcu, L. Protesescu, S. Yakunin, M. I. Bodnarchuk, M. J. Grotevent, M. V. Kovalenko, *Nano Lett.* **2015**, *15*, 5635.

[22] J. Song, J. Li, X. Li, L. Xu, Y. Dong, H. Zeng, *Adv. Mater.* **2015**, *27*, 7162.

[23] Y. H. Kim, H. Cho, J. H. Heo, T. S. Kim, N. Myoung, C. L. Lee, S. H. Im, T. W. Lee, *Adv. Mater.* **2015**, *27*, 1248.

[24] R. L. Hoye, M. R. Chua, K. P. Musselman, G. Li, M. L. Lai, Z. K. Tan, N. C. Greenham, J. L. MacManus-Driscoll, R. H. Friend, D. Credgington, *Adv. Mater.* **2015**, *27*, 1414.

[25] G. Li, Z.-K. Tan, D. Di, M. L. Lai, L. Jiang, J. H.-W. Lim, R. H. Friend, N. C. Greenham, *Nano Lett.* **2015**, *15*, 2640.

[26] J. Li, S. G. R. Bade, X. Shan, Z. Yu, *Adv. Mater.* **2015**, *27*, 5196.

[27] Y. Ling, Z. Yuan, Y. Tian, X. Wang, J. C. Wang, Y. Xin, K. Hanson, B. Ma, H. Gao, *Adv. Mater.* http://dx.doi.org/10.1002/adma.201503954.

[28] A. Dualeh, N. Tétreault, T. Moehl, P. Gao, M. K. Nazeeruddin, M. Grätzel, *Adv. Funct. Mater.* **2014**, *24*, 3250.

[29] J. C. Yu, D. B. Kim, G. Baek, B. R. Lee, E. D. Jung, S. Lee, J. H. Chu, D. K. Lee, K. J. Choi, S. Cho, M. H. Song, *Adv. Mater.* **2015**, *27*, 3492.

[30] J. C. Yu, D. B. Kim, E. D. Jung, B. R. Lee, M. H. Song, *Nanoscale* http://dx.doi.org/10.1039/c5nr05604g.

[31] H. Cho, S.-H. Jeong, M.-H. Park, Y.-H. Kim, C. Wolf, C.-L. Lee, J. H. Heo, A. Sadhanala, N. Myoung, S. Yoo, S. H. Im, R. H. Friend, T.-W. Lee, *Science* **2015**, *350*, 1222.

[32] C. Bi, Y. C. Shao, Y. B. Yuan, Z. G. Xiao, C. G. Wang, Y. L. Gao, J. S. Huang, *J. Mater. Chem. A* **2014**, *2*, 18508.

[33] W. L. Ma, C. Y. Yang, X. Gong, K. Lee, A. J. Heeger, *Adv. Funct. Mater.* **2005**, *15*, 1617

[34] C.-J. Hsu, H.-S. Duan, W. Yang, H. Zhou, Y. Yang, *Adv. Energy Mater.* **2014**, *4*, 1301287.

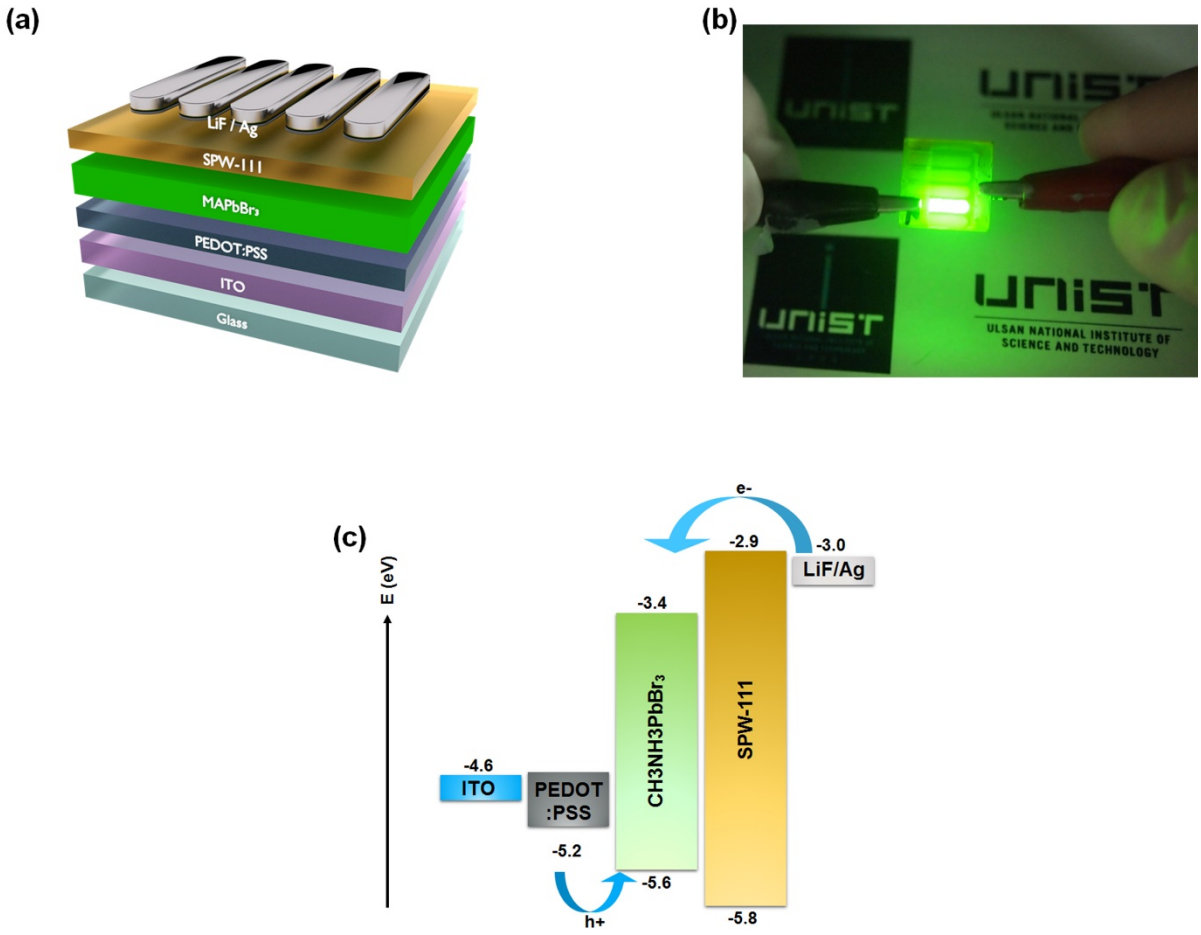

Figure 1. (a) The device structure of the PeLED (ITO/PEDOT:PSS/$MAPbBr_3$/SPW-111/LiF/Ag); (b) the green EL from the PeLED with an $MAPbBr_3$ film annealed at 60 °C for 2 hrs; and (c) energy levels of the various device components in the PeLED.

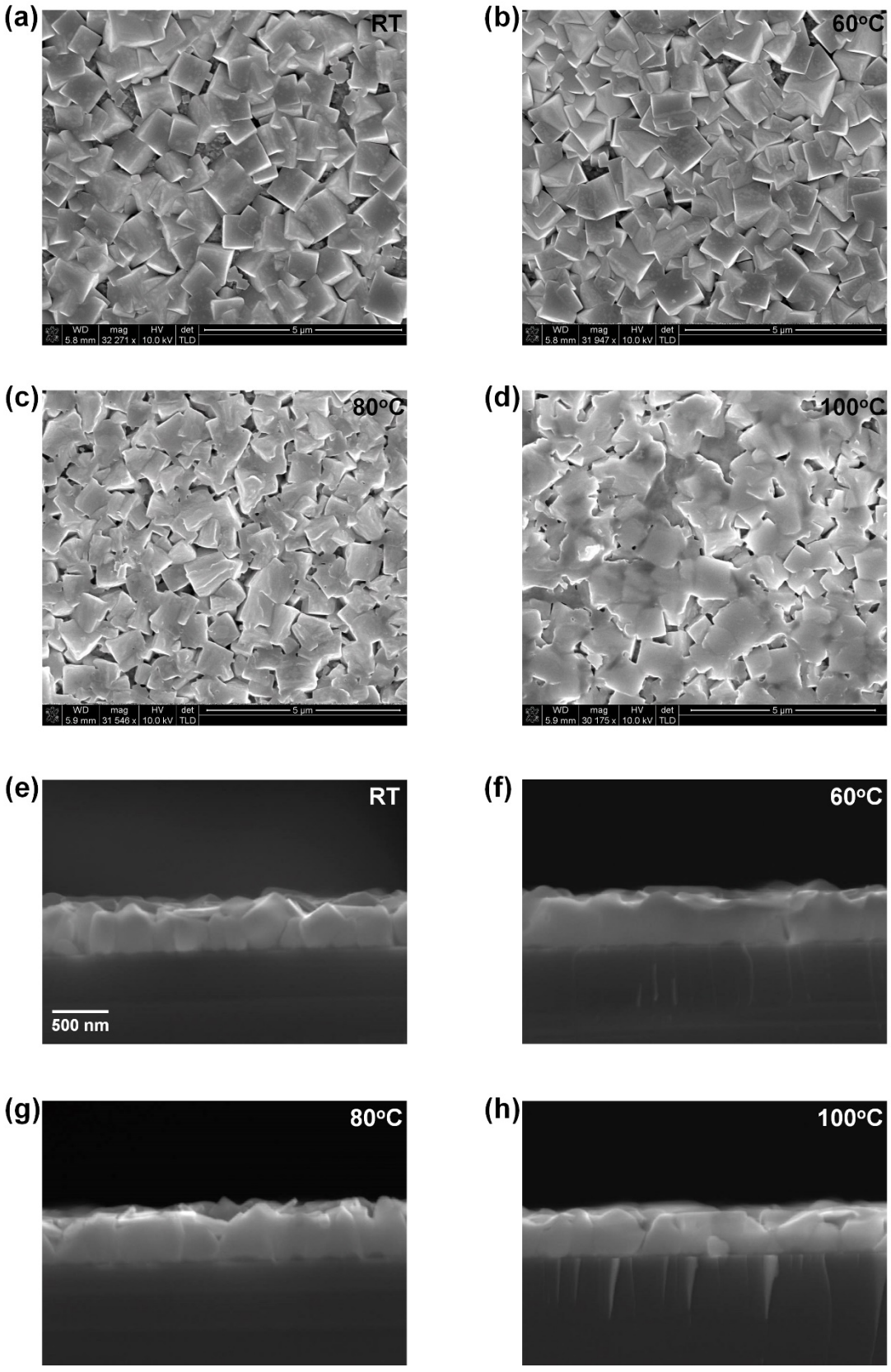

Figure 2. (a)-(d) The top-surface and (e)-(h) the cross section of the $MAPbBr_3$ films treated at various temperatures (RT, 60 °C, 80 °C and 100 °C) for 2 hrs.

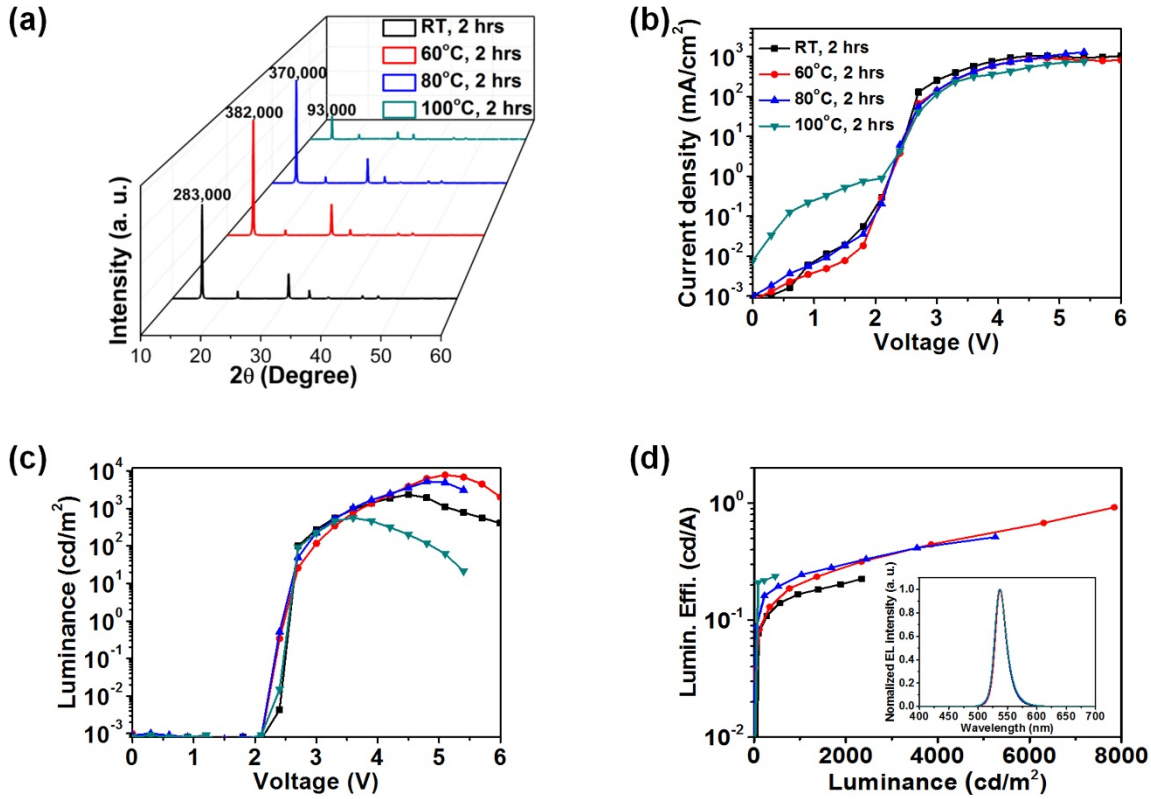

Figure 3. (a) XRD patterns of the $MAPbBr_3$ films treated at different temperatures (RT, 60 °C, 80 °C and 100 °C) for 2 hrs, wherein the $MAPbBr_3$ films were deposited onto PEDOT:PSS-coated ITO/glass substrates. Light-emitting characterization of the PeLEDs with an $MAPbBr_3$ film treated at different temperatures (RT, 60 °C, 80 °C and 100 °C) for 2 hrs in terms of (b) current density vs. voltage (*J*-*V*), (c) luminance vs. voltage (*L*-*V*), and (d) luminous efficiency vs. luminance (*LE*-*L*). The figure inset shows the EL spectra from the PeLED.

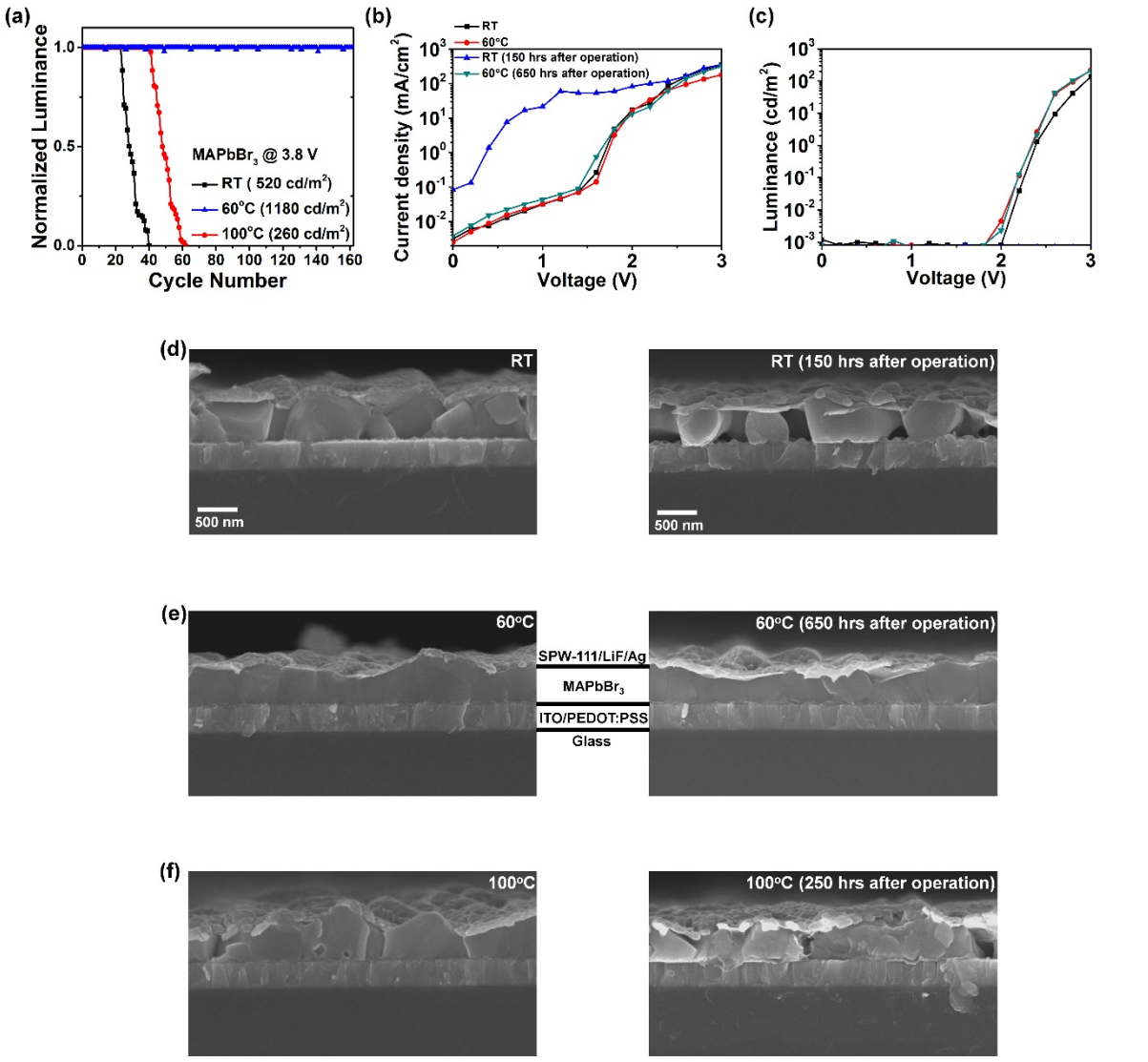

Figure 4. (a) The long-term stability of encapsulated PeLEDs with an $MAPbBr_3$ film treated at different temperatures (RT, 60 °C, 80 °C and 100 °C) for 2 hrs were evaluated in terms of normalized luminance under ambient atmospheric conditions. The procedure for long-term stability measurements is given as follows: the luminance of the encapsulated PeLEDs was measured, and the tested PeLEDs were stored in a glovebox for 4 hrs, representing a single cycle. (b) Current density vs. voltage (*J*-*V*) and (c) luminance vs. voltage (*L*-*V*) of the PeLED with an $MAPbBr_3$ film annealed at RT and 60 °C for 2 hrs before and after operation. (d)-(f) Cross-sectional SEM images of the complete PeLEDs with an $MAPbBr_3$ film treated at different temperatures (RT, 60 °C, and 100 °C) for 2 hrs before and after operation (37 (150 hrs), 67 (250 hrs), and 162 cycles (650 hrs)).

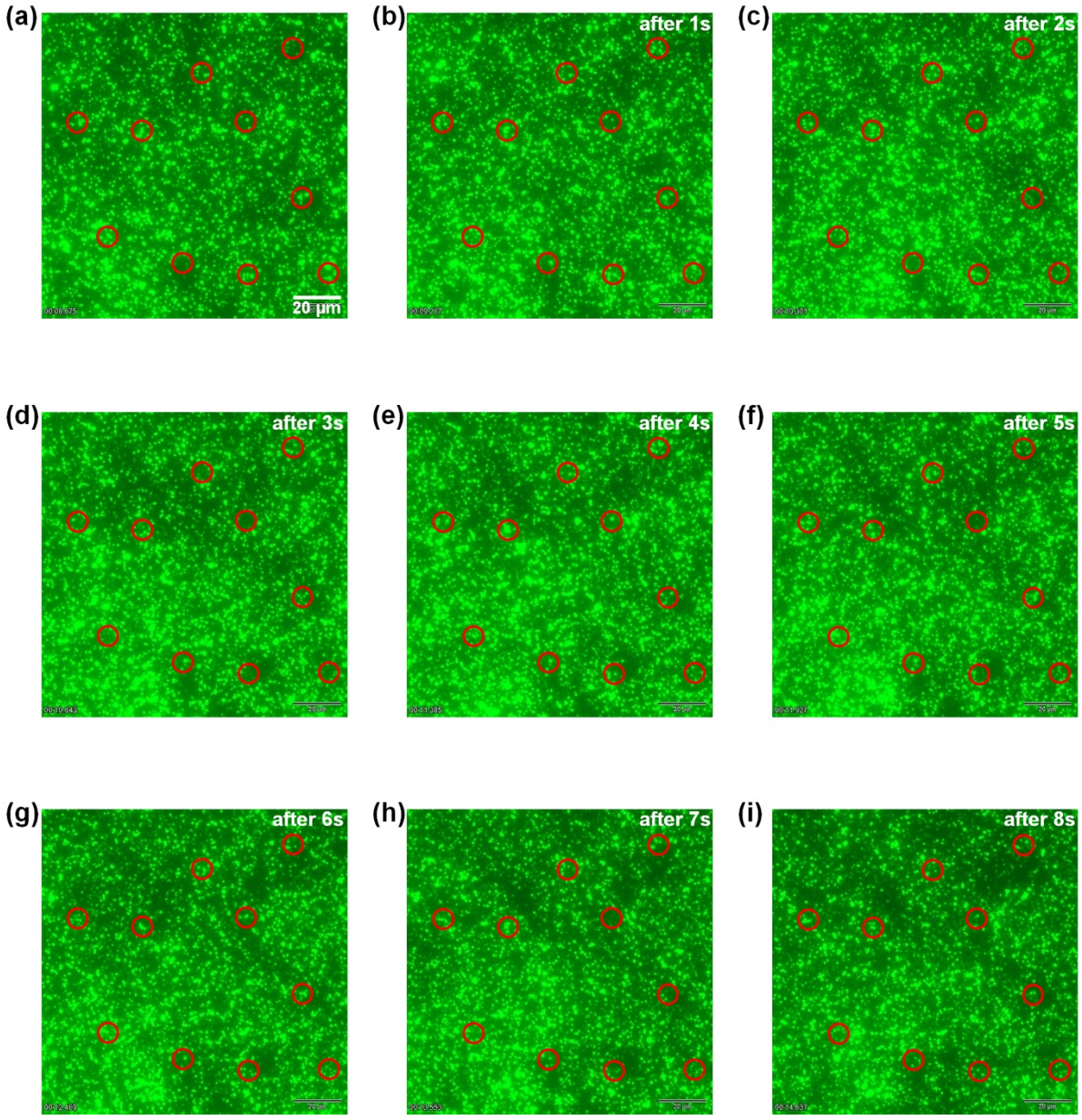

Figure 5. Time-dependent of the EL behavior of the PeLED with $MAPbBr_3$ film annealed at 60 ^{o}C under constant 3.4 V. The microscope images were taken total 100 frames for 10 s. The selected frames are shown with selected red circles to illustrate the changing pattern of emission with time.

Table 1. Summary of the device performance of PeLEDs with $MAPbBr_3$ treated at different temperature for 2 hrs.

Devices configuration (ITO/PEDOT:PSS/$MAPbBr_3$/SPB-02T/LiF/Ag)	L_{max} [cd/m^2] @ bias	LE_{max} [cd/A] @ bias	PE_{max} [lm/W] @ bias	EQE_{max} [%] @ bias
Storage time (2 hrs, RT)	2,350 @ 4.5	0.23 @ 4.5	0.16 @ 4.5	0.05 @ 4.5
Annealing time (2 hrs, 60 °C)	7,850 @ 5.1	0.92 @ 5.1	0.57 @ 5.1	0.20 @ 5.1
Annealing time (2 hrs, 80 °C)	5,250 @ 4.8	0.51 @ 4.8	0.34 @ 4.8	0.12 @ 4.8
Annealing time (2 hrs, 100 °C)	550 @ 3.6	0.19 @ 3.0	0.20 @ 3.0	0.04 @ 3.0

Table of contents entry

Keyword: perovskite; perovskite light-emitting diodes (PeLED); long-term stability; electroluminescence (EL)

*Jae Choul Yu, Dae Woo Kim, Da Bin Kim, Eui Dae Jung, Jong Hyun Park, Ah-Young Lee, Daniele Di Nuzzo, Richard H. Friend and Myoung Hoon Song**

Improving the Stability and Performance of Perovskite Light-Emitting Diodes by Thermal Annealing Treatment

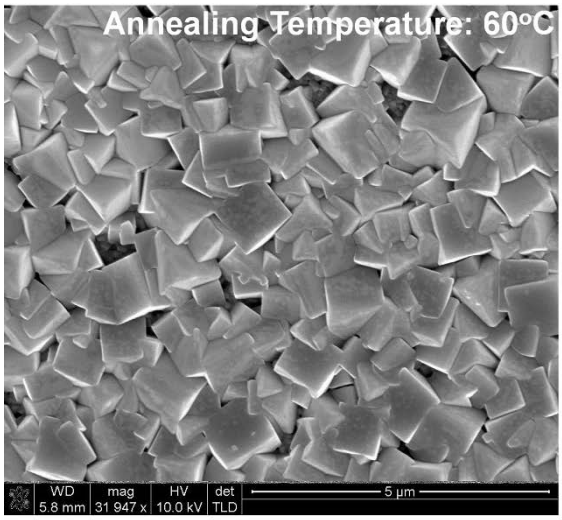

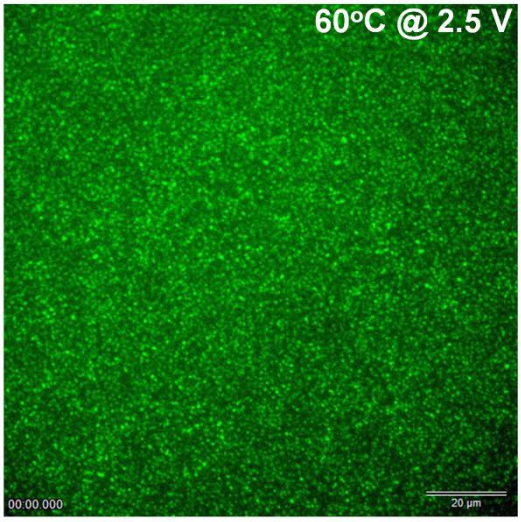

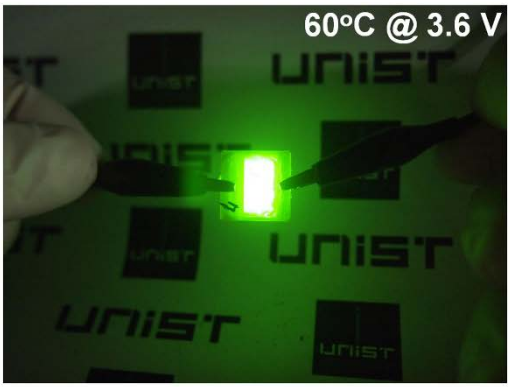

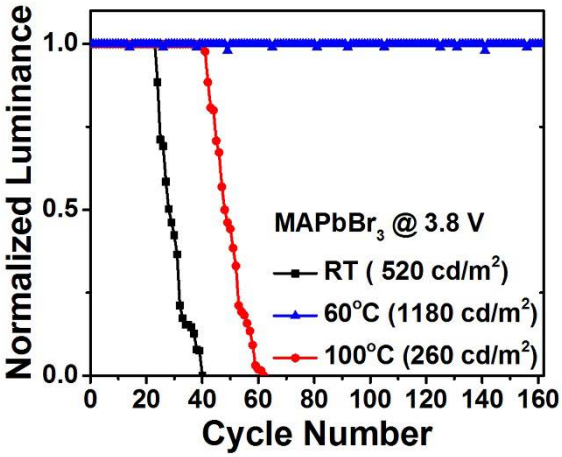

Submitted to ADVANCED MATERIALS

Copyright WILEY-VCH Verlag GmbH & Co. KGaA, 69469 Weinheim, Germany, 2013.

Supporting Information

for *Adv. Mater.*, DOI: 10.1002/adma.

Improving the Stability and Performance of Perovskite Light-Emitting Diodes by Thermal Annealing Treatment

*Jae Choul Yu, Dae Woo Kim, Da Bin Kim, Eui Dae Jung, Jong Hyun Park, Ah-Young Lee, Daniele Di Nuzzo, Richard H. Friend and Myoung Hoon Song**

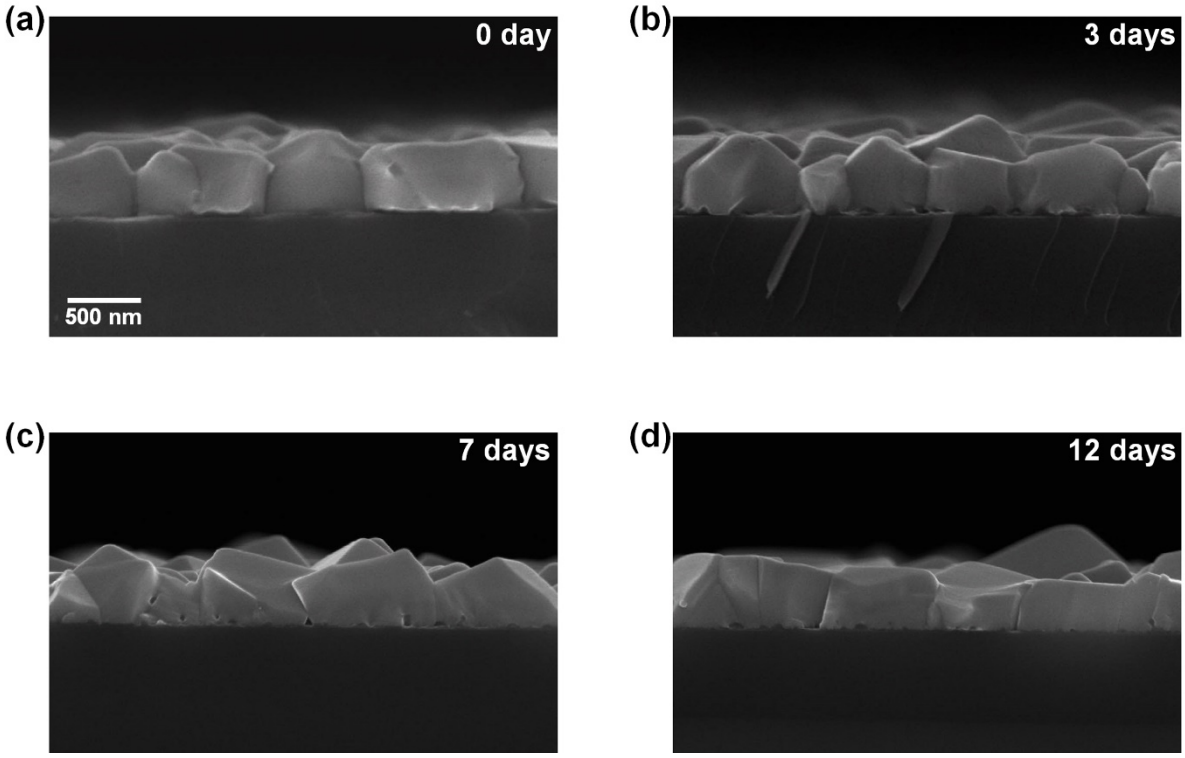

Figure S1. Cross sectional SEM images of (a)-(d) the $MAPbBr_3$ films with different storage times in N_2-filled glovebox (0 ~ 12 days).

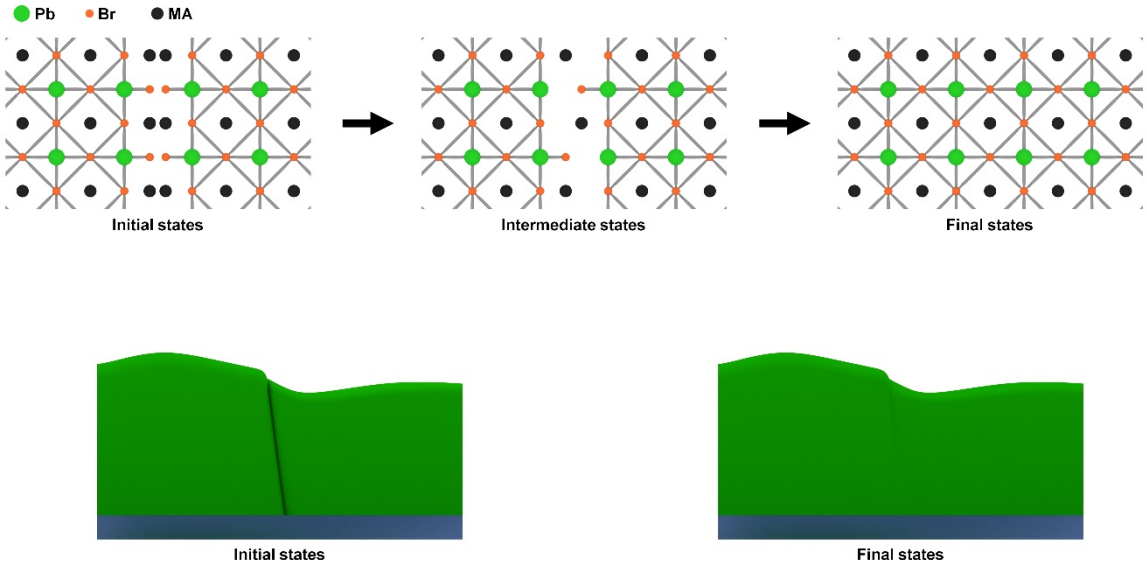

Figure S2. Schematic diagram of connection of perovskite film during storage in glovebox.

We speculate that this result arises from a reduction in the energy of the perovskite crystal surface, as shown in **Figure S2**. If the $MAPbBr_3$ crystals are assumed to consist of a $[PbBr_6]^{4-}$ octahedral unit cell, the bromide (Br) atoms are dominant at the $MAPbBr_3$ crystal surface, as shown in **Figure S2**a. However, a spontaneously connected $MAPbBr_3$ film is expected to reduce the overall surface energy at the $MAPbBr_3$ crystal surface after being stored for several days, as shown in **Figure S2**c. We used energy-dispersive spectrometry (EDS) to determine the molar ratio between Pb and Br in the $MAPbBr_3$ films stored for different times in the N_2-filled glove box; the results support the hypothesis of a connected $MAPbBr_3$ film. As expected, the molar ratio of Pb to Br in the $MAPbBr_3$ films approaches 1/3 after storage in the N_2-filled glove box for 7 days (see **Table S1**), which agrees well with the reduction of the Br-rich surface area in the perovskite crystal.

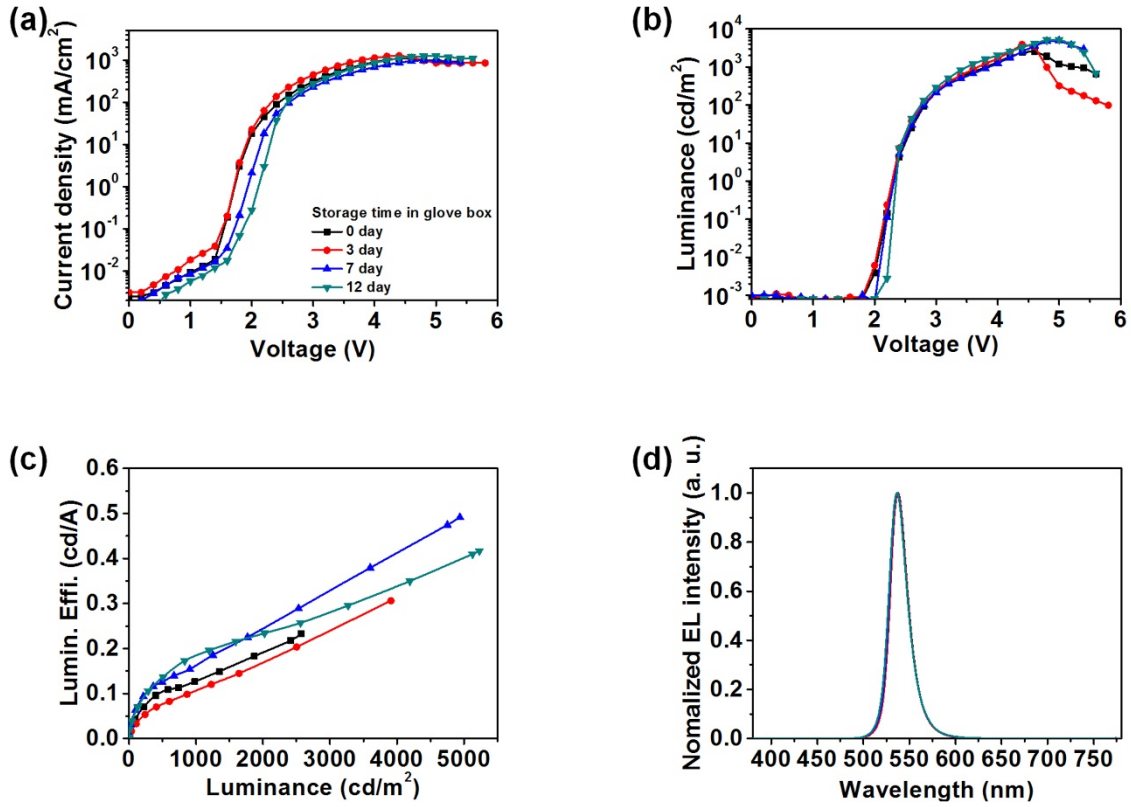

Figure S3. Light-emitting charactarization of PeLEDs with $MAPbBr_3$ films for different storage times in terms of (a) current density vs. voltage (*J*-*V*), (b) luminance vs. voltage (*L*-*V*), (c) luminous efficiency vs. luminance (*LE*-*L*), and (d) EL spectra.

To determine the correlation between the continuous $MAPbBr_3$ film and device performance, we tested PeLEDs fabricated with $MAPbBr_3$ films stored for different times in the N_2-filled glove box; the results are presented in **Figure S3**. The reference device without storage presented a maximum luminance of 2,560 cd m^{-2} (at 4.6 V) and a luminous efficiency of 0.21 cd A^{-1} (at 4.4 V). By contrast, the PeLED with an $MAPbBr_3$ film stored for 7 days in the N_2-filled glove box exhibited a remarkably improved maximum luminance of 4,940 cd m^{-2} (at 5.0 V) and a luminous efficiency of 0.49 cd A^{-1} (at 5.0 V), which were improvements of 190 % and 230 %, respectively, compared with those of the reference PeLED. The detailed device performance values of the PeLEDs are summarized in **Table S2**. The enhanced performance of the PeLED with a continuous perovskite film motivated us to further explore the effect of the morphology of the perovskite film on device performance. To investigate whether the composition of the $MAPbBr_3$ crystal changed after storage in the N_2-filled glove box, we conducted EDS measurements. The initial $MAPbBr_3$ film exhibited a Pb/Br molar ratio of 0.27, which implied a Br-rich surface. If the obtained $MAPbBr_3$ films are assumed to consist of an ideal $[PbBr_6]^{4-}$ octahedral unit cell, then Br atoms should account for a large percentage of the surface,

as shown in **Fig. S2**a. However, the spontaneously connected $MAPbBr_3$ film is expected to reduce the overall surface energy at the $MAPbBr_3$ crystal surface, thereby resulting in a Pb/Br molar ratio approximately equal to the optimal value of 1/3 for $MAPbBr_3$ after storage in the N_2-filled glove box for 7 days.

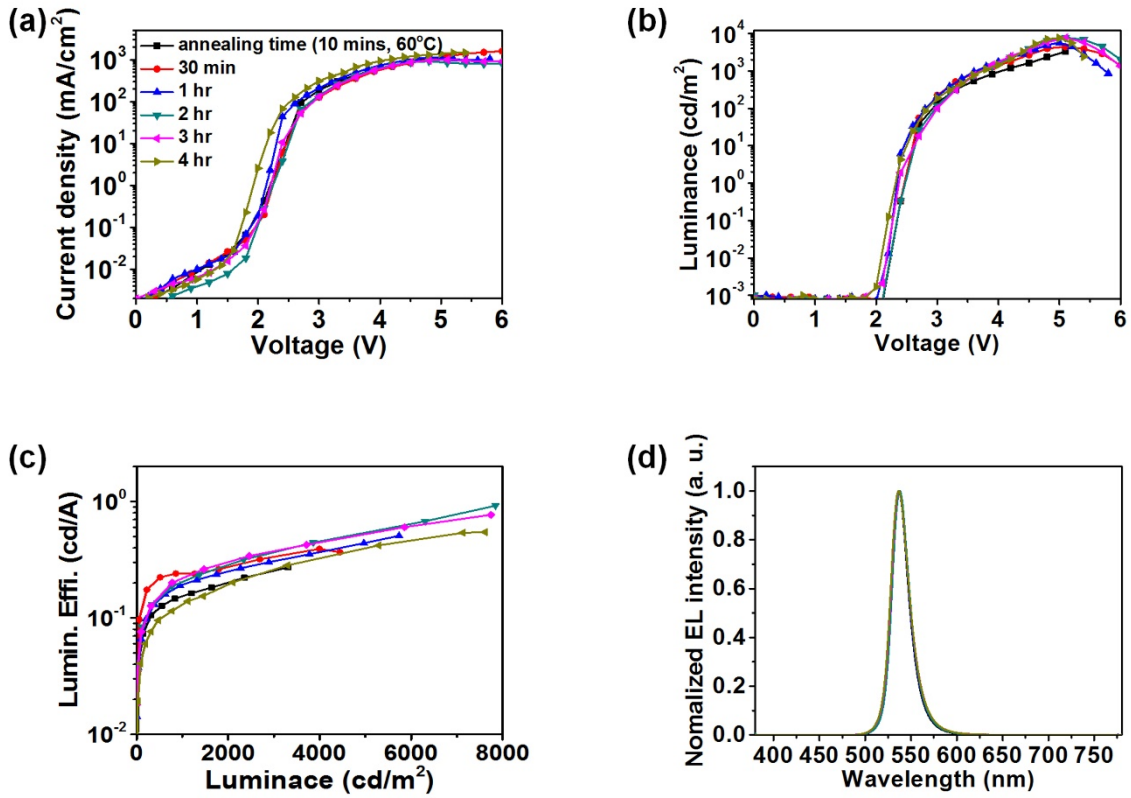

Figure S4. Light-emitting charactarization of PeLEDs with $MAPbBr_3$ films annealed at 60 ^{o}C for different annealing times in terms of (a) current density vs. voltage (*J*-*V*), (b) luminance vs. voltage (*L*-*V*), (c) luminous efficiency vs. luminance (*LE*-*L*), and (d) EL spectra.

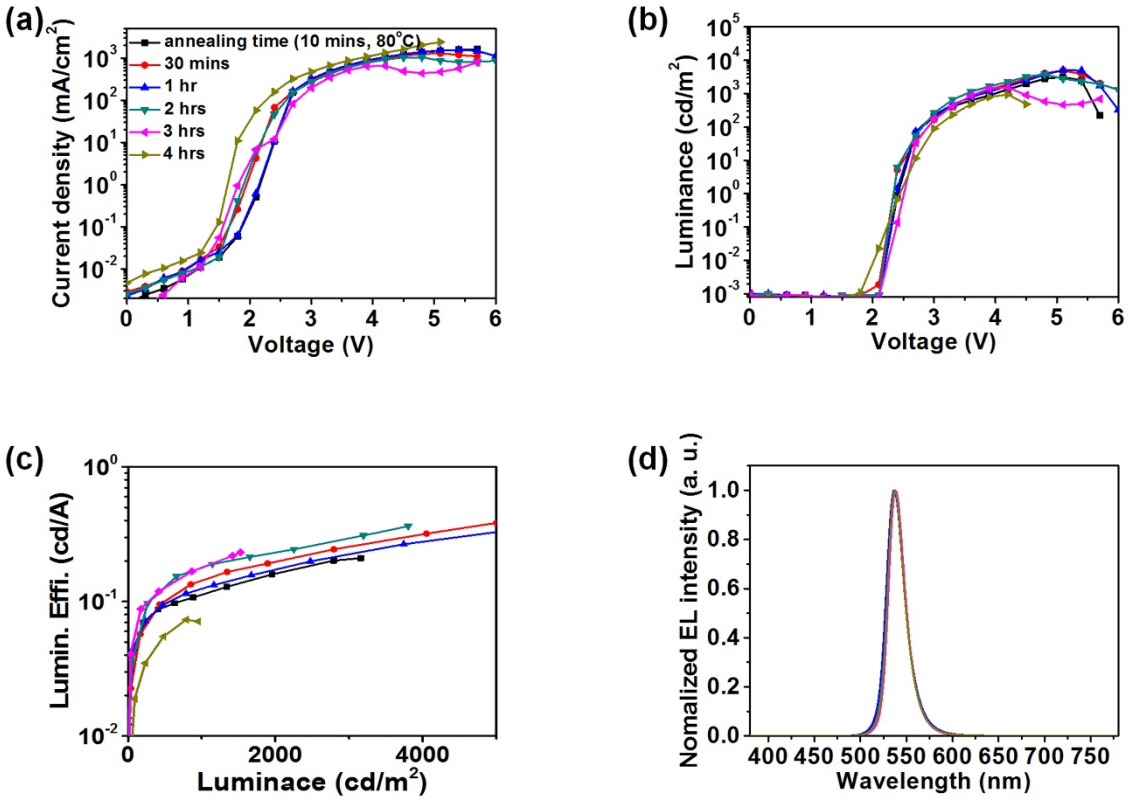

Figure S5. Light-emitting charactarization of PeLEDs with $MAPbBr_3$ films annealed at 80 ^oC for different annealing times in terms of (a) current density vs. voltage (J-V), (b) luminance vs. voltage (L-V), (c) luminous efficiency vs. luminance (LE-L), and (d) EL spectra.

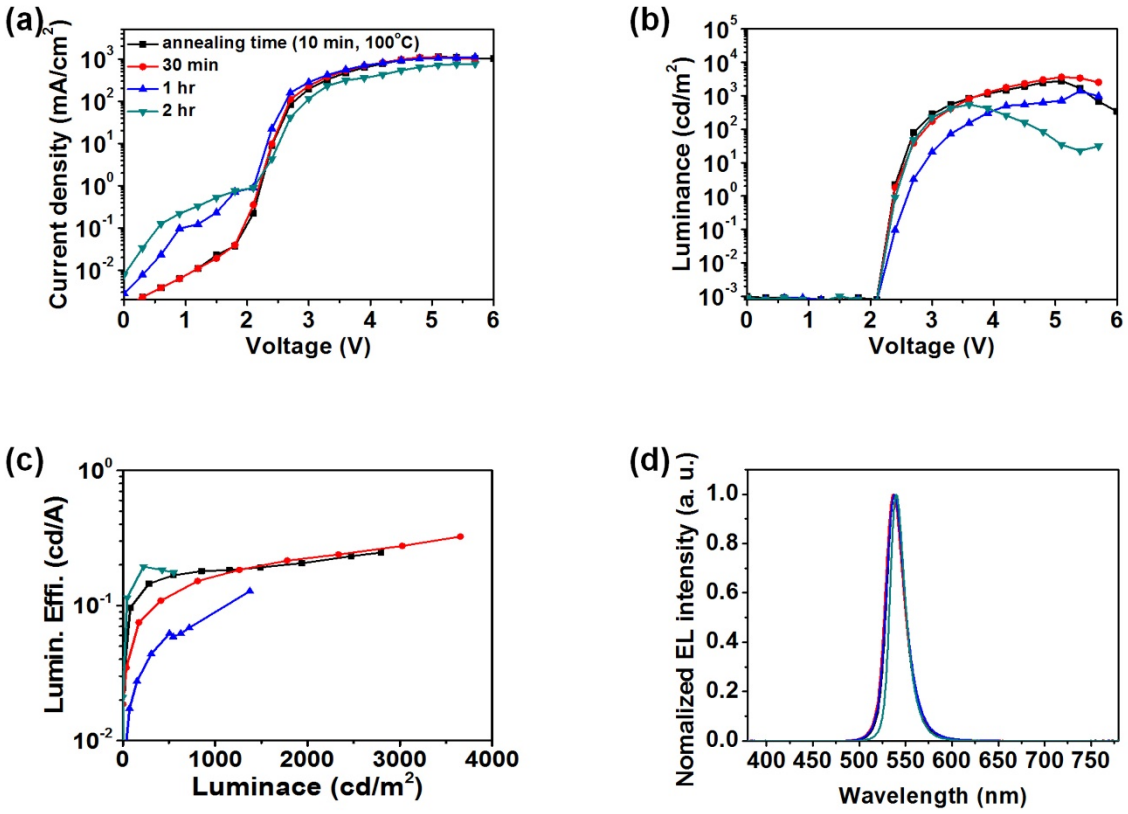

Figure S6. Light-emitting charactarization of PeLEDs with $MAPbBr_3$ films annealed at 100 ^oC for different annealing times in terms of (a) current density vs. voltage (J-V), (b) luminance vs. voltage (L-V), (c) luminous efficiency vs. luminance (LE-L), and (d) EL spectra.

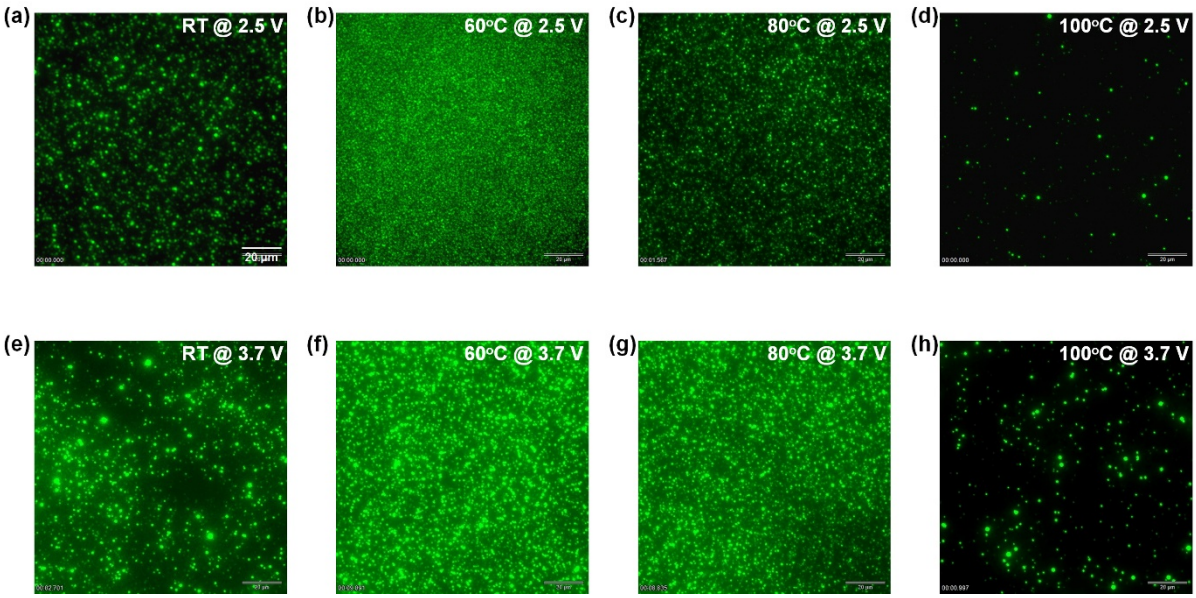

Figure S7. Inverted optical microscope images of EL from PeLEDs with $MAPbBr_3$ films annealed at different temperature for 2 hrs under turn-on voltage (at 2.5 V) and operation voltage (at 3.7 V).

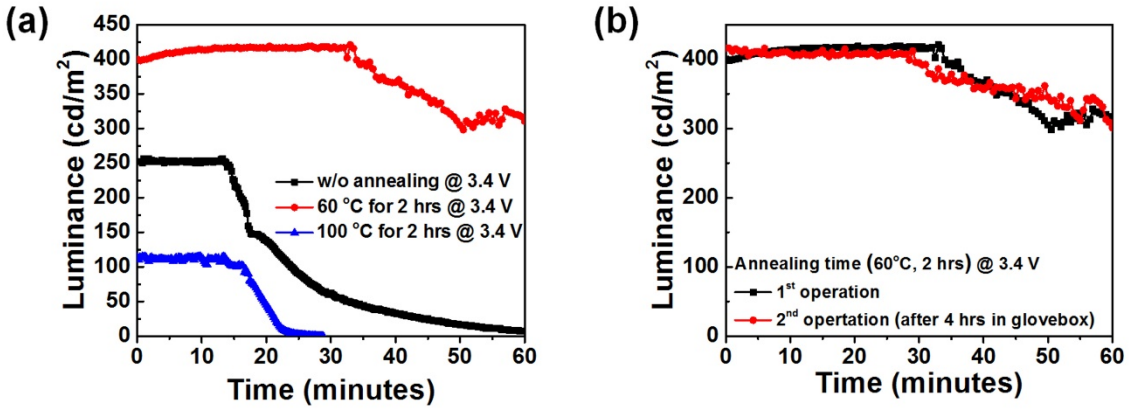

Figure S8. (a) Luminance characteristics of PeLEDs with $MAPbBr_3$ films annealed at RT, 60 ^oC and 100 ^oC for 2 hrs under constant bias. (b) Luminance characteristics of PeLED with MAPbBr3 films annealed at 60 oC before and after storage in the glovebox for 4 hrs.

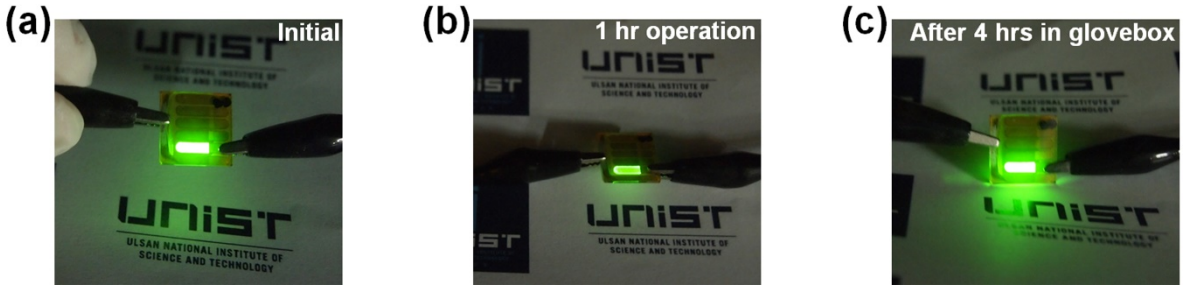

Figure S9. Photographs of the green emission from the PeLED at 3.4 V (a) before, (b) after 1 hr operation and (c) after storage in the glovebox for 4 hrs, respectively.

Table S1. Bromide and lead molar ratio of $MAPbBr_3$ films with different storage times in N_2-filled glove box determined by applying EDS characterization.

After day	Br (%)	Pb (%)
0	78.7	21.3
3	77.5	22.5
7	76.5	23.5
12	76.7	23.3

Table S2. Summary of the device performances of PeLEDs with $MAPbBr_3$ films after different storage times in N_2-filled glove box.

Devices configuration (ITO/PEDOT:PSS/$MAPbBr_3$ /SPB-02T/LiF/Ag)	L_{max} [cd/m^2] @ bias	LE_{max} [cd/A] @ bias	PE_{max} [lm/W] @ bias	EQE_{max} [%] @ bias
0 day	2,560 @ 4.6	0.21 @ 4.4	0.15 @ 4.4	0.05 @ 4.6
3 days	3,910 @ 4.4	0.31 @ 4.4	0.22 @ 4.4	0.07 @ 4.4
7 days	4,940@ 5.0	0.49 @ 5.0	0.31 @ 4.8	0.11 @ 5.0
12 days	5,230 @ 5.0	0.42 @ 5.0	0.27 @ 4.8	0.09 @ 5.0

Table S3. Carbon, bromide and lead weigh percent of $MAPbBr_3$ films annealed at 60 ^oC and 100 ^oC for 2hrs determined by applying EDS characterization.

Annealing Time, Temp.	Carbon (wt. %)	Bromide (wt. %)	Lead (wt. %)
60^{o}C, 2 hrs	6.34	12.01	6.43
100^{o}C, 2 hrs	4.08	7.95	6.40

Table S4. Summary of the device performances of PeLEDs with $MAPbBr_3$ annealed at 60 ^oC for different annealing times.

Devices configuration (ITO/PEDOT:PSS/$MAPbBr_3$/SPB-02T/LiF/Ag)	L_{max} [cd/m^2] @ bias	LE_{max} [cd/A] @ bias	PE_{max} [lm/W] @ bias	EQE_{max} [%] @ bias
Annealing time (10 mins, 60^oC)	3,310 @ 5.1	0.26 @ 4.8	0.17 @ 4.8	0.06 @ 4.8
30 mins	4,450 @ 5.1	0.39 @ 4.8	0.26 @ 4.8	0.09 @ 4.8
1 hr	5,740 @ 5.0	0.51 @ 5.0	0.32 @ 5.0	0.12 @ 5.0
2 hrs	7,850 @ 5.1	0.92 @ 5.1	0.57 @ 5.1	0.20 @ 5.1
3 hrs	7,740 @ 5.1	0.77 @ 5.1	0.47 @ 5.1	0.17 @ 5.1
4 hrs	7,610 @ 5.0	0.55 @ 5.0	0.35 @ 5.0	0.12 @ 5.0

Table S5. Summary of the device performances of PeLEDs with $MAPbBr_3$ annealed at 80 ^oC for different annealing times.

Devices configuration (ITO/PEDOT:PSS/$MAPbBr_3$/SPB-02T/LiF/Ag)	L_{max} [cd/m^2] @ bias	LE_{max} [cd/A] @ bias	PE_{max} [lm/W] @ bias	EQE_{max} [%] @ bias
Annealing time (10 mins, 80^oC)	3,160 @ 5.1	0.21 @ 5.1	0.13 @ 4.8	0.05 @ 5.1
30 mins	5,000 @ 5.1	0.38 @ 5.1	0.24 @ 5.1	0.08 @ 5.1
1 hr	5,080 @ 5.1	0.33 @ 5.1	0.20 @ 5.1	0.07 @ 5.1
2 hrs	3,800 @ 4.8	0.36 @ 4.8	0.26 @ 4.8	0.08 @ 4.8
3 hrs	1,530 @ 4.2	0.23 @ 4.2	0.17 @ 4.2	0.05 @ 4.2
4 hrs	950 @ 4.2	0.07 @ 3.9	0.06 @ 3.9	0.02 @ 3.9

Table S6. Summary of the device performances of PeLEDs with $MAPbBr_3$ annealed at 100 ^oC for different annealing times.

Devices configuration (ITO/PEDOT:PSS/$MAPbBr_3$/SPB-02T/LiF/Ag)	L_{max} [cd/m^2] @ bias	LE_{max} [cd/A] @ bias	PE_{max} [lm/W] @ bias	EQE_{max} [%] @ bias
Annealing time (10 mins, 100^oC)	2,790 @ 5.1	0.25 @ 5.1	0.15 @ 5.1	0.05 @ 5.1
30 mins	3,660 @ 5.1	0.32 @ 5.1	0.20 @ 5.1	0.07 @ 5.1
1 hr	1,380 @ 5.4	0.13 @ 5.4	0.07 @ 5.4	0.03 @ 5.4
2 hrs	550 @ 3.6	0.19 @ 3.0	0.20 @ 3.0	0.04 @ 3.0